ACS APPLIED MATERIALS & INTERFACES

Research Article

www.acsami.org

Green in Situ Synthesis of Clean 3D Chestnutlike Ag/WO_{3-x} Nanostructures for Highly Efficient, Recyclable and Sensitive SERS Sensing

Jian Huang,[†] Dayan Ma,[‡] Feng Chen,[†] Dongzhen Chen,[†] Min Bai,[†] Kewei Xu,[‡,§] and Yongxi Zhao*[,†]

[†]Key Laboratory of Biomedical Information Engineering of Education Ministry, School of Life Science and Technology, Xi'an Jiaotong University, Xi'an, Shaanxi 710049, P. R. China

[‡]State Key Laboratory for Mechanical Behavior of Materials, School of Materials Science and Engineering, Xi'an Jiaotong University, Xi'an, Shaanxi 710049, P. R. China

[§]Xi'an University, Xi'an, Shaanxi 710065, P. R. China

Supporting Information

ABSTRACT: Surface-enhanced Raman scattering (SERS) has proven to be an effective technique for identifying and providing fingerprint structural information on various analytes in low concentration. However, this analytical technique has been plagued by the ubiquitous presence of organic contaminants on roughened SERS substrate surfaces, which not only often result in poorer detection sensitivity but also significantly affect the reproducibility and accuracy of SERS analysis. Herein, we developed a clean, stable, and recyclable three-dimensional (3D) chestnutlike Ag/WO_{3-x} ($0 < x < 0.28$) SERS substrate by simple hydrothermal reaction and subsequent green in situ decoration of silver nanoparticles. None of the organic additives were used in synthesis, which ensures the substrate surfaces are completely clean and free of interferences from impurities. The innovative design combines the SERS enhancement effect and self-cleaning property, making it a multifunctional and reusable SERS platform for highly sensitive SERS detection. Using malachite green as a model target, the as-prepared SERS substrates exhibited good reproducibility (relative standard deviation of 7.5%) and pushed the detection limit down to 0.29 pM. The enhancement factor was found to be as high as 1.4×10^7 based on the analysis of 4-aminothiophenol. The excellent regeneration performance indicated that the 3D biomimetic SERS substrates can be reused many times. In addition, the fabricated substrate was successfully employed for detecting thiram in water with a detection limit of 0.32 nM, and a good linear relationship was obtained between the logarithmic intensities and the logarithmic concentrations of thiram ranging from 1 nM to 1 μM. More importantly, the resultant SERS-active colloid can be used for accurate and reliable determination of thiram in real fruit peels. These results predict that the proposed SERS system have great potential toward rapid, reliable, and on-site analysis, especially for food safety and environmental supervision.

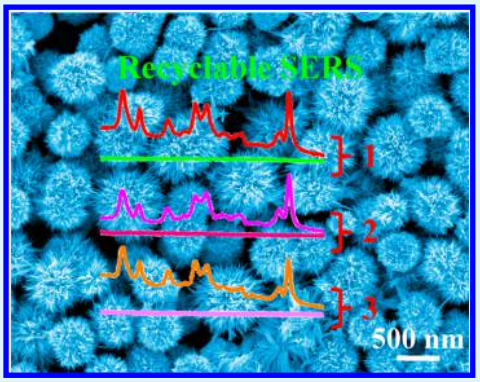

KEYWORDS: *chestnutlike, Ag/WO_{3-x}, green, recyclable, surface-enhanced Raman scattering*

1. INTRODUCTION

Surface-enhanced Raman scattering (SERS) has been rapidly developed and widely applied in many fields due to its high sensitivity and specificity.[1−8] Recently, a large number of SERS substrates with various microstructures and morphologies have been designed and fabricated successfully.[9−21] Particularly, three-dimensional (3D) hierarchical nanostructures with special morphologies and unique properties have attracted considerable attention.[22−29] They not only have a large specific surface area which can adsorb more probe molecules and be beneficial to the improvement of SERS sensitivity but also have the potential to further expand the arrangement of hotspots along the third dimension.[30−33] Generally, most of the 3D hierarchical nanostructures are made from pure noble metallic nanostructures or noble-metal nanoparticles composites with different template scaffolds such as nanowire arrays,[34,35] porous channels,[22,36] oriented nanorods,[37] and core−shell nanosphere et al. Considering the economic feasibility and application versatility, the 3D hierarchical noble metal/template scaffolds hybrid nanostructures have drawn intensive attention in the field of sensing and catalysis.[38]

In the synthesis of noble metal/template scaffolds hybrid nanostructures, the key strategy is the use of specific compounds such as coupling agents, surfactants, reductants, polymers, and other functional organic agents. These additives act as terminating or stabilizing agents to decrease growth rate, prevent interparticle agglomeration, and improve stability and processability. However, they lead to the presence of an organic

Received: November 14, 2016
Accepted: February 8, 2017
Published: February 8, 2017

DOI: 10.1021/acsami.6b14571
ACS Appl. Mater. Interfaces 2017, 9, 7436−7446

Scheme 1. Schematic Illustration of the Fabrication Process of the 3D Recyclable Chestnutlike Ag/WO_{3-x} ($0 < x < 0.28$) Nanostructures and Its Application: (I) Ag NPs Decorated on $WO_{2.72}$ Nanochestnuts, (II) Analyte Loading and SERS Sensing, and (III) the Regeneration of Recyclable SERS Substrates

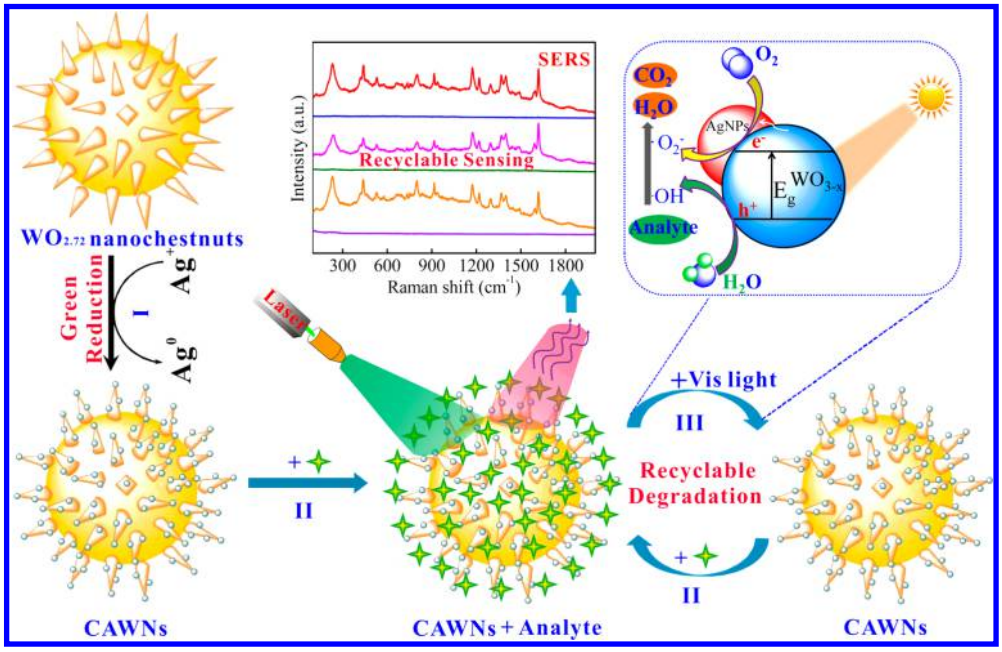

layer contamination on the surface of the 3D hybrid nanostructures. Importantly, these organic layers may often diminish the plasmonic activity of the original metal nanoparticles and easily cause a loss of probe binding site.[39] Besides, they may bring extra interferential bands in the SERS measurements, especially if the target analytes have similar Raman spectral response with the additives. The bad contact between noble metal and template scaffolds also leads to uncertainties in regard to improving the efficiency of charge separation and transport. Unfortunately, the cleaning and elimination of the organic layers is very difficult and costly. Therefore, it becomes crucial to devise a green strategy for achieving the clean surface without additives and at a lower cost.

Alternatively, if the noble metal could be directly grown onto the supports, the clean surface of metal/template scaffolds would exhibit a tremendously improved background and the SERS sensitivity would also be significantly enhanced.[40] For most types of transition metal oxides, their low valence state or nonstoichiometric species are often found to have weak reducing power.[41] The reductive oxide could then react with the oxidative noble-metal salt in aqueous solution without any additives.[42] By this in situ redox reaction, it should be possible to grow noble metal particles directly on the oxide surface, such as Au or Ag nanoparticles (Ag NPs).

The fresh $WO_{2.72}$ as a nonstoichiometric semiconductor, its surface can also provide the necessary reduction potential to facilitate the formation of uniform Ag NPs. In this process, the $WO_{2.72}$ serves as both the source of electrons that reduce the Ag ion in solution and the template scaffolds for Ag NPs. The density and average size of the Ag NPs are strictly dependent on metal salt concentration and deposition time. Furthermore, recent studies have shown that $WO_{2.72}$ can be used as effective photocatalysts for the degradation of organic pollutants. It would be a very innovative design if we can combine photocatalytic degradation characteristics and SERS performance in a clean 3D hierarchical Ag/WO_{3-x} ($0 < x < 0.28$) nanostructure substrate. Unfortunately, there are no reports yet about the fabrication of clean, stable, and recyclable 3D $WO_{2.72}$-based SERS substrates.

On the basis of the above considerations, here, we report a simple and green route to synthesize the recyclable 3D chestnutlike Ag/WO_{3-x} ($0 < x < 0.28$) nanostructures (CAWNs) by a hydrothermal method and subsequent in situ redox reaction. No foreign reducing agents or other additives are required, avoiding the introduction of impurities and ensuring that the surfaces of 3D CAWNs SERS substrates are clean. The clean surfaces with high-density Ag NPs exhibited a significant improved background signal and a considerable increase of Raman signal for SERS sensing. For example, based on the high-density hotspots and clean surfaces of the 3D hierarchy, the resulting hybrid CAWNs have been used for ultrasensitive detection of malachite green (MG) with a detection limit of 0.29 pM. Meanwhile, the pesticide thiram with a low concentration of 0.32 nM can readily be determined via the SERS chip ascribed to its superior SERS enhancement and clean surfaces, much lower than the maximum residue limits (MRLs) of thiram (0.01−0.1 mg/kg). More significantly, the prepared CAWNs colloid is also demonstrated to be highly suitable for determination of thiram in various real fruit peels. Furthermore, the decoration of Ag NPs on the surface of nonstoichiometric $WO_{2.72}$ successfully realized the recycling of SERS substrate (Scheme 1). The recyclability of SERS substrates and the corresponding mechanisms of photocatalytic degradation are preliminary discussed. Owing to oxygen-vacancy-rich $WO_{2.72}$, scaffolds will be oxidized preferentially compared with Ag NPs, which provides many more opportunities for the protection of Ag NPs. As a clean, stable, recyclable SERS substrate, this platform can also be applied to many other target analytes, thus prompting the practical exploitation of SERS sensing.

DOI: 10.1021/acsami.6b14571
ACS Appl. Mater. Interfaces 2017, 9, 7436−7446

2. EXPERIMENTAL SECTION

Chemicals and Materials. Tungsten hexachloride (WCl_6), 4-aminothiophenol (4-ATP), and thiram were purchased from Aladdin Industrial Corporation in Shanghai, silver nitrate ($AgNO_3$) and absolute ethanol (CH_3CH_2OH) were purchased from China National Pharmaceutical Group Corporation, malachite green (MG) was purchased from Dongjiang Chemicals Company, and silicon wafer was purchased from the Luoyang Single Crystal Silicon Corporation. All chemicals were used as received without further purification. Double-distilled water (>18.0 MΩ cm) was used throughout the experiments. The pericarps were peeled from fruits which were purchased from the local supermarket.

Synthesis of Nonstoichiometric $WO_{2.72}$ Nanostructures. $WO_{2.72}$ nanostructures with different morphology on the Si/SiO_2 substrate were prepared according to the hydrothermal approach. A certain quality of tungsten hexachloride (from 0.1 to 3 g) was dissolved in 80 mL absolute ethanol and was transferred to a Teflon-lined stainless steel autoclave. The autoclave was then sealed and heated at 180 °C for 24 h. After finishing the reaction, the reactor was cooled to room temperature; the samples were rinsed thoroughly with ethanol and double-distilled water and dried naturally at room temperature.

Synthesis of 3D CAWNs with Optimal Ag NPs. Ag NPs were deposited on the as-prepared nonstoichiometric $WO_{2.72}$ by a facile in situ redox at room temperature. About 0.4 g of the as-synthesized $WO_{2.72}$ sample was added into 80 mL distilled water under continuous stir. About 2 mL $AgNO_3$ aqueous solution with different concentrations (from 0.01 to 0.1 M) was dropped into the $WO_{2.72}$ suspension twice (0.5 mL $AgNO_3$ was added within 4 h and then another 1.5 mL added subsequently). With continuous stirring for 12 h, the final product was collected, washed carefully with ethanol and double-distilled water, and then dried by nitrogen flow for further applications. Other detailed experimental procedures and fully characterized data were given in the Supporting Information.

Characterization. The morphology and the structure of the as-fabricated samples were characterized by field emission scanning electron microscope (FE-SEM, Hitachi SU6600), transmission electron microscope (TEM,JEM-2100F), and X-ray diffraction (XRD, with Cu Kα radiation, Bruker D8 Advanced). Ultraviolet−visible (UV−vis) spectra were performed on a Hitachi U-4100 spectrophotometer.

SERS Measurements. Raman measurements were performed on a Horiba HR 800 confocal microprobe Raman system at room temperature with a 633 nm laser. The laser spot area was ∼1 μm in diameter and the incident power was 1.7 mW. The data acquisition time was 10 s for one accumulation unless otherwise specified. Thiram and MG were selected as the probe molecule for SERS measurement. For SERS EF evaluation, 10 μL 4-ATP aqueous solutions were dropped onto the referencing substrate and SERS substrate for data acquisition.

Detections of Thiram and MG in Water Using Self-Assembled SERS Substrates. The poorly water-soluble thiram pesticide was first dissolved in organic solvent. Briefly, 1 mM thiram solution in ethanol was prepared and diluted with water to the predetermined concentrations. Then the thiram solution with different concentrations was dropped onto the self-assembled SERS substrates. The Raman spectra were recorded using a 633 nm laser with 1.7 mW powers and an objective lens (∼1 μm spot). The acquisition time is 10 s and slit aperture is 50 μm unless otherwise noted. Owing to its excellent water solubility, the MG powder was dissolved in water and diluted into different concentrations. The SERS detections of MG in water were performed using the same procedure.

Direct Detections of Thiram in Fruit Peels Using SERS-active Nanocolloid. The Raman technique for the detection of thiram pesticides at fruit peels (orange and carambola) was demonstrated here. The thin peels were taken from fruits using a knife and formatted to a uniform disk piece with a standard metal punch of ∼5 mm diameter. The thiram solution with different concentrations was spiked into various fruit peels (the spiked peels were prepared by the addition of 20 μL of pesticide solution with different concentrations to cover the overall surface of peels and were completely dried at room temperature). Generally, the pesticide residues either adsorb at the surface of fruit peels or permeate into the inner of peels. Before detection of pesticides, 20 μL of ethanol was first dropped to the surface of spiked peel and naturally evaporated to dryness. Subsequently, 20 μL of concentrated Ag/WO_{3-x} nanoparticle colloid was added to the above peels and until the colloid nearly dried (before used, the dilute Ag/WO_{3-x} colloid was concentrated for achieving a higher particle density at fruit peels). The active Ag/WO_{3-x} nanoparticles will be located at the surface of peels and closely be in contact with or adsorb the target species. Finally, the peels were placed onto the Raman measurement platform for data acquisition.

Recyclability Characterization (Visible Light Photocatalytic Degradation of MG or Thiram). For recyclability characterization, the fresh Ag/WO_{3-x} colloid was first concentrated and drop-casted onto the preprocessed Si wafer (or Si/SiO_2 wafer). After the SERS measurement, the substrates were rinsed with deionized water for 5 s and then subjected to visible light irradiation for 50 min (equipped with a 1000 W xenon lamp and the wavelength from 400 to 800 nm). The light source was positioned approximately 5 cm from the top of the sample holder, which was fan-cooled during the experiment. The UV high pressure mercury lamp (300 W, 365 nm) is also equipped for other application. The irradiated substrates were rinsed by deionized water for another 5 s to remove the residual ions and drying by nitrogen blowing at room temperature. Finally, the substrates were employed again to detect MG or thiram under the same experimental conditions as the first time.

3. RESULTS AND DISCUSSION

3.1. Preparation and Characterization of $WO_{2.72}$ Suboxide. WO_{3-x} as a new kind of transition metal oxide has attracted considerable attention owing to its unusual defect structure and unique properties. In particular, the non-stoichiometric suboxide $WO_{2.72}$ has the largest oxygen deficiency and extraordinary chemical properties. It also can be easily separated from other tungsten oxides and were employed as photocatalyst, electrode material, photothermal therapeutic agent, and so on.

For the preparation, three kinds of $WO_{2.72}$ nanostructures with different morphologies (nanowires, nanowires bundles, and chestnutlike nanostructures, Figure 1) were synthesized by hydrothermal method using tungsten hexachloride (WCl_6) and ethanol without any additives. Our experimental results suggest that a low precursor concentration (C_{WCl6} < 0.01 M) contributes to the formation of large-scale $WO_{2.72}$ nanowires with large aspect ratio and lengths of up to several micrometers (Figure 1, a1−a2). However, when the precursor concentration varies between 0.01 and 0.04 M, the nanowires packed together in the form of bundled nanowires (Figure 1, b1−b2). Interestingly, the chestnutlike micronanospheres composed of numerous nanotips were obtained (with larger diameters ∼800 nm) at higher concentration (C_{WCl6} > 0.04 M, Figure 1, c1−c2).

Energy-dispersive X-ray spectroscopy (EDS) confirms that the as-prepared sample contains W and O elements (Figure 2a). X-ray diffraction (XRD) displays the typical diffraction peaks that are consistent to monoclinic suboxide $WO_{2.72}$ with lattice constants of a = 18.3, b = 3.78, and c = 14.0 Å (Figure 2b). It is clear that four diffraction peaks at 2θ of 23.4°, 34.9°, 47.8°, and 55.2° correspond to the (010), (204), (020), and (204) lattice plane of monoclinic $WO_{2.72}$, respectively. The representative Raman spectrum is acquired for distinguishing the different phases of tungsten oxides, which agrees well with the general characteristics of $WO_{2.72}$ (Figure 2c). These results indicate that the synthesized nanostructures were the oxygen-

DOI: 10.1021/acsami.6b14571
ACS Appl. Mater. Interfaces 2017, 9, 7436−7446

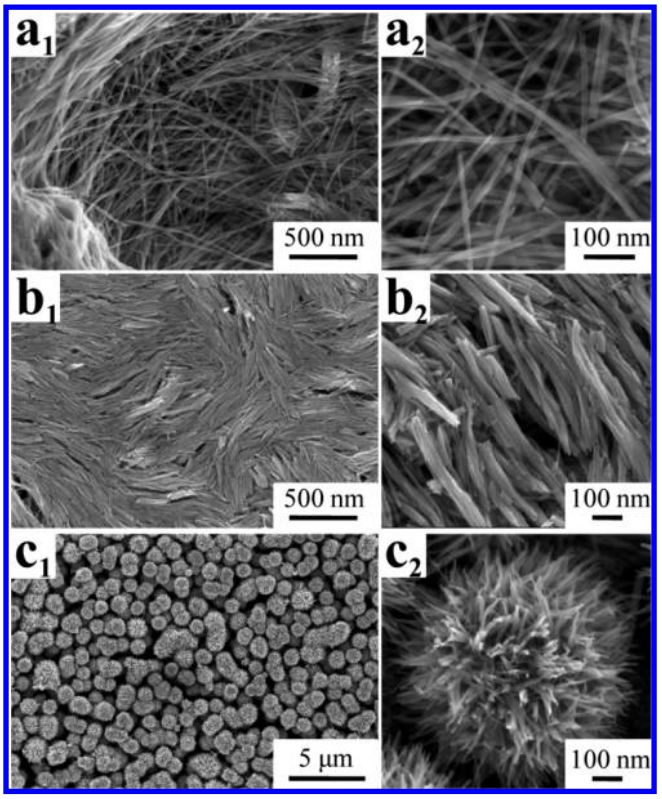

Figure 1. SEM images of the as-prepared $WO_{2.72}$ suboxide nanostructures: (a1−a2) nanowires, (b1−b2) nanowires bundles, and (c1−c2) 3D nanochestnuts at different magnifications.

vacancy-rich $WO_{2.72}$. Also, we can estimate their specific surface area by monitoring the weight loss of moisture (viz thermogravimetry analysis). That is to say, the larger specific surface area corresponds to the higher loss-in-weight of absorbed moisture. In Figure 2d, the thermal behavior of 3D nanochestnuts implies large adsorption capacity ascribing to its high specific surface area, which is a favorable factor for SERS detection and photocatalysis.[42] Besides, the proposed formation process and hydrothermal mechanism had been analyzed and discussed (details were shown in Part I). Importantly, using the synthesized pure $WO_{2.72}$ nanostructures as the substrate material, rhodamine 6G (R6G) as a probe molecule, the detection limit was as low as 10^{-7} M and the maximum enhancement factor was 3.4×10^5. This enhancement performance and detection capability was in the rank of the high sensitivity among semiconducting materials, even comparable to noble metals without hot spots.[43] It would be a very helpful design if we combined the substoichiometric $WO_{2.72}$ nanostructure (which has already been shown with strong SERS activity) and high-density noble metals with abundant hot spots in the 3D hierarchical noble metals/semiconducting WO_{3-x} composite SERS substrates.

3.2. Synthesis of 3D Chestnutlike Ag/WO_{3-x} Nanostructures (CAWNs). Recently, the synthesis of 3D semiconductor structures coupled with noble metal nanoparticles might be a promising candidate for photocatalysis and fabrication of SERS substrates.[44] The UV−vis absorption spectrum of 3D chestnutlike $WO_{2.72}$ nanostructure is shown in Figure S1. A considerable absorption tail emerged in the visible and near-infrared regions (400−1100 nm), which gives clear evidence that the nonstoichiometric suboxide $WO_{2.72}$ contains a large number of oxygen vacancies. Surprisingly, the presence of oxygen vacancies makes $WO_{2.72}$ have mild reducing power. We could observe that reductive chestnutlike $WO_{2.72}$ reacts with $AgNO_3$ solution at room temperature without any additives (the pure $WO_{2.72}$ undecorated with Ag NPs was used as a reference in Figure 3, panels a−b). As shown in Figure 3, panels c−d, SEM shows that high-density Ag NPs with uniform size and spacing are distributed evenly throughout the $WO_{2.72}$ scaffolds. The Ag element is further confirmed by the energy dispersive spectroscopy (EDS) analysis (Figure 3, e−h) and TEM (Figure S2). Obviously, the STEM-EDS mapping and TEM also shows that the Ag NPs are decorated evenly on the reducing $WO_{2.72}$ scaffolds. Owing to the freshly prepared $WO_{2.72}$ providing the necessary reduction potential for the decoration of Ag NPs, once the silver ions were reduced into Ag NPs, the outer surfaces of $WO_{2.72}$ were oxidized into WO_3

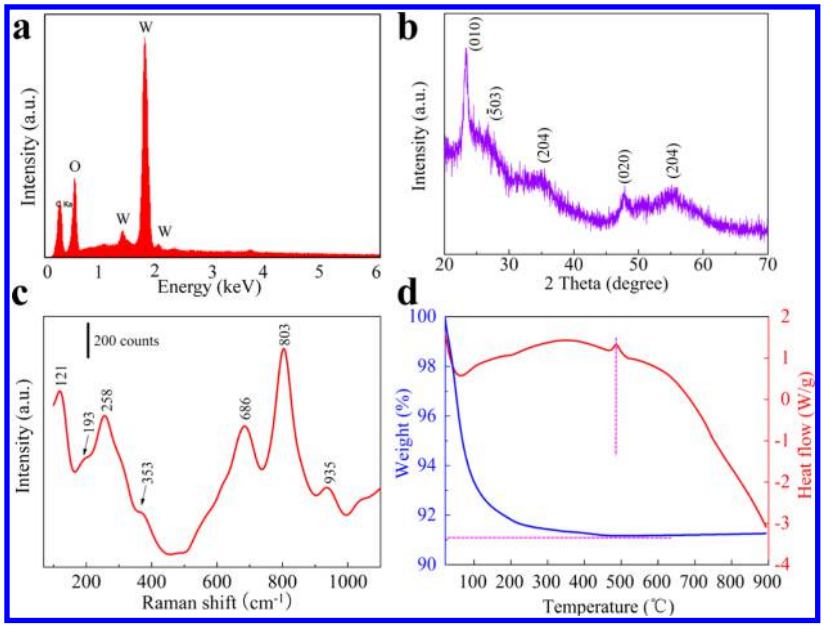

Figure 2. Characterization of the as-prepared 3D $WO_{2.72}$ suboxide samples: (a) EDS, (b) XRD pattern, (c) Raman spectrum, and (d) TG analysis.

DOI: 10.1021/acsami.6b14571
ACS Appl. Mater. Interfaces 2017, 9, 7436−7446

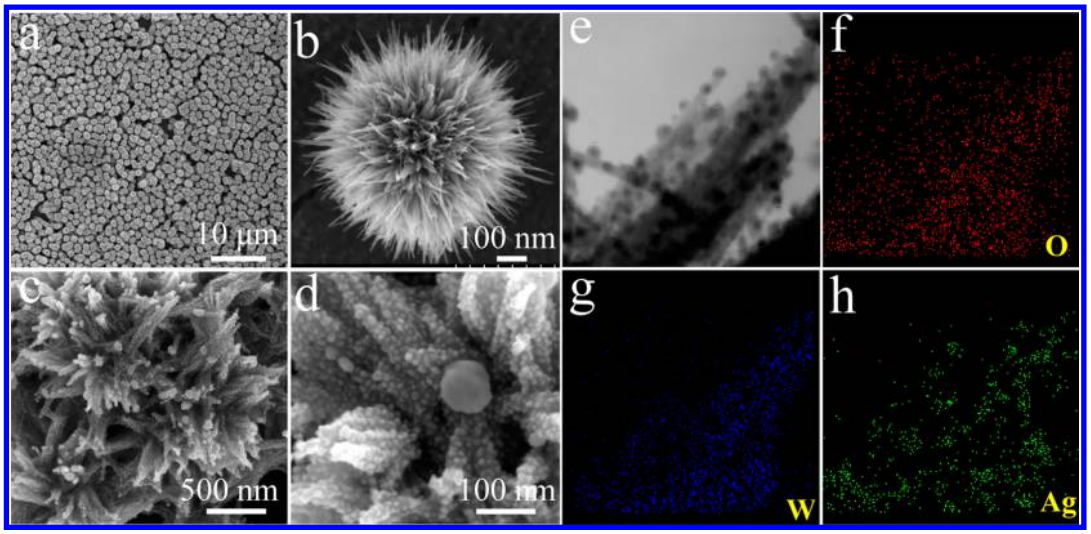

Figure 3. (a–b) The representative SEM images of the formed 3D chestnutlike $WO_{2.72}$ nanostructures, (c–d) SEM images of Ag NPs decorated $WO_{2.72}$ nanochestnuts, (e) selected image of the 3D Ag/WO_{3-x} nanostructures for the EDS mapping analysis, and (f, g, and h) represent the element mapping O, W, and Ag, respectively.

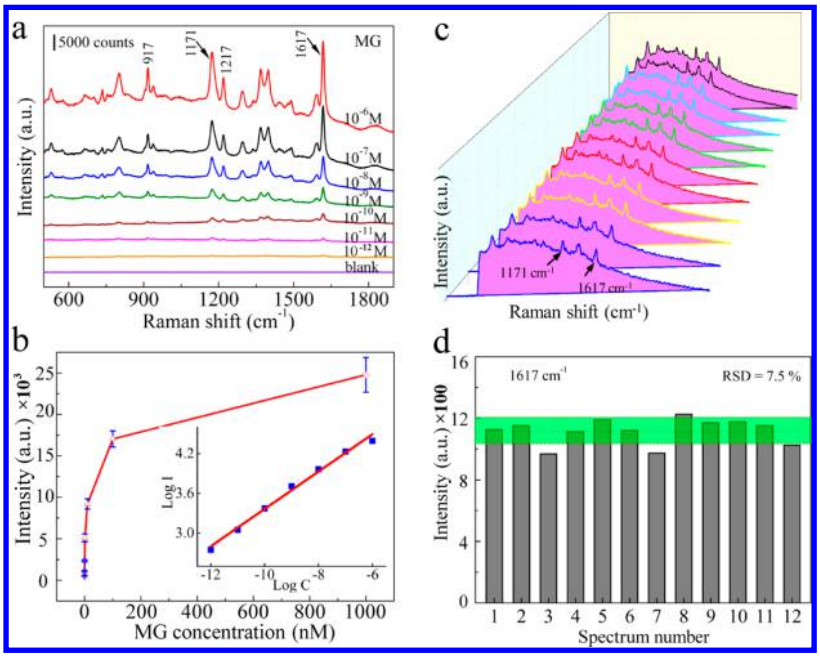

Figure 4. Results for the quantitative detection of MG, (a) concentration-dependent SERS spectra for MG detection at various concentrations on substrates, (b) plot of the peak intensity at 1617 cm^{-1} as a function of MG concentration, the inset represents the linear relationship from 10^{-12} M to 10^{-6} M. Reproducibility and uniformity of the as-prepared SERS substrates with 10^{-11} M MG adsorbed on the surface, (c) represent the SERS spectra collected at 12 random dots, and (d) represent variation of SERS intensity at the specific Raman modes of 1617 cm^{-1}.

gradually, and then a thin layer of WO_3 would form and adjoin the Ag NPs. This is similar to the galvanic displacement between the germanium nanowires and $AgNO_3$. According to the infrared spectroscopic analysis, we can also estimate the surface is clean and without any absorbed molecule except for water.[42]

The Ag NPs were successfully decorated on the three kinds of $WO_{2.72}$ nanostructures and then self-assembled into 1D, 2D, or 3D SERS substrates, respectively (Figure S3). However, the great differences were observed in SERS activity (Figure S4). The 3D hierarchical nanochestnut exhibits higher SERS enhancement because of the large surface area (which can adsorb a large number of probe molecules) and high-density Ag NPs along the third dimension. Besides, the optimal size of the Ag NPs can be tuned by varying the deposition time or concentration of $AgNO_3$ solution (Figure S5). The results clearly demonstrated that the most suitable size is not the smallest/largest one for obtaining the maximum SERS enhancement (Figure S6). More importantly, the Ag NPs were directly grown on $WO_{2.72}$ without any additives. The totally clean interfaces can effectively reduce the noise of the Raman detection, thereby realizing sensitive and rapid detection without complex cleaning steps (Figure S7). Meanwhile, more probe molecules could be adsorbed on the clean interfaces owing the decrease of stereohindrance effect and the increase of adsorption sites. In order to understand the interactions between the electromagnetic wave and the as-prepared 3D CAWNs substrates, the finite difference time

DOI: 10.1021/acsami.6b14571
ACS Appl. Mater. Interfaces 2017, 9, 7436–7446

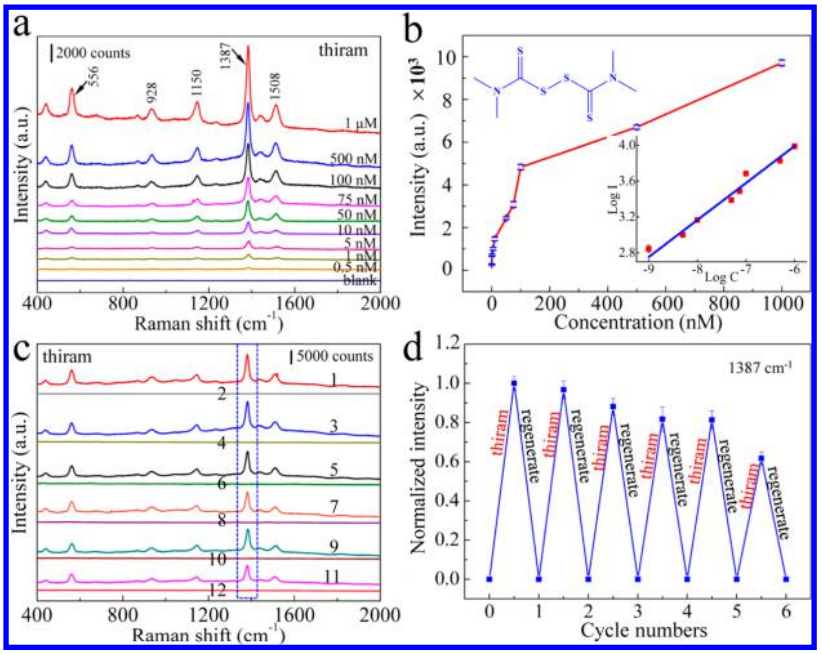

Figure 5. Results for the quantitative detection of thiram and regeneration test, (a) concentration-dependent SERS spectra for thiram detection at various concentrations on substrates, (b) plot of the peak intensity at 1387 cm^{-1} as a function of thiram concentration (inset represents the linear relationship from 10^{-9} M to 10^{-6} M), (c) SERS spectra of thiram before and after self-cleaning test, and (d) corresponding normalized Raman intensities of 1387 cm^{-1} when the SERS substrate chip is recycling for six times in the detection of 1 μM thiram.

domain (FDTD) method was also applied for calculations (for details, see Part II in the Supporting Information). The simulation results demonstrated a relatively homogeneous 3D electromagnetic field distribution in CAWNs because of the presence of a larger number of 3D hierarchical scaffolds and the high-density Ag NPs.

3.3. Evaluating SERS Activity of CAWNs Substrates. To evaluate the SERS enhancement and analytical capability of the assembly 3D CAWNs substrates, the detection of MG (a forbidden triphenylmethane dye in aquaculture that has been reported causing carcinogenesis, mutagenesis, and chromosomal fractures) was carried out by combining a qualitative and quantitative way. Simply, a series of MG gradient concentrations are prepared and dropped onto the well-optimized SERS substrates. As the solvent evaporated, the representative Raman spectra were collected successively from 10^{-12} to 10^{-6} M (Figure 4a). It is highly acceptable for Raman signal recognition, and the main fingerprint peaks in each spectrum can be facilely identified. For example, four main characteristic bands were clearly seen at 917, 1171, 1217, and 1617 cm^{-1} (the detailed assignments for these bands were shown in Table S1). The obvious enhancements were also found until an extreme dilute solution (10^{-12} M), which was a just detectable concentration (the magnified view was shown in Figure S8).

A calibration curve based on the concentration of MG and the Raman intensity of the peak at 1617 cm^{-1} is shown in Figure 4b. At certain concentrations (from 10^{-12} M to 10^{-6} M), the logarithmic curve shows excellent linearity. The calibrated linear regression equation is $\log I_{1617} = (0.282 \pm 0.005) \log C_{MG} + (6.180 \pm 0.050)$, with a squared correlation coefficient (R^2) of 0.9915 (inset of Figure 4b). The limit of detection (LOD) based on a signal-to-noise of 3 (S/N = 3) was estimated to be as low as 2.9×10^{-13} M of MG, with an excellent linearity of 10^{-12}–10^{-6} M, demonstrating a higher sensitivity and a wider quantitation range than other conventional detection means. Such detection sensitivity is high enough for MG determination in common biochemical and environmental samples.

Besides the high sensitivity, the uniformity and reproducibility is also an important prerequisite for SERS detection. Twelve different spots on the as-prepared substrates were chosen for Raman measurements (Figure 4c). The relative standard deviation (RSD) at 1617 cm^{-1} and at 1171 cm^{-1} is about 7.5% and 7.8%, respectively (Figure 4d and Figure S9), indicating excellent uniformity and high reproducibility of the as-prepared substrates.[30] Owing to their uniformity and reproducibility, the SERS substrates can be cut into small pieces for detecting trace chemical or biological molecules and the utilization of substrates would be improved dramatically. Furthermore, 4-aminothiophenol (4-ATP) was used as a model Raman probe to evaluate the enhancement factor (EF).[45] The EF at the peak of 1079 cm^{-1} of 4-ATP was calculated to be 1.4×10^7 for the CAWNs substrates (details were given in the Supporting Information, Part III). The calculated EF is more than 10^7, indicating excellent electromagnetic enhancement, which is sufficiently high to offer ultrasensitive and nondestructive characterization of target analytes by the localized surface plasmon resonance (LSPR).

3.4. Regenerability of CAWNs Substrates. The 3D CAWNs metal/semiconductor materials can be not only used for SERS detection but also used for the degradation of the adsorptive analytes. Upon irradiated under visible light, the excited CAWNs will reduce the dissolved/adsorbed molecular oxygen into a superoxide radical, which will then generate highly active oxidative species such as $\bullet O_2^-$ and $\bullet$OH. These oxidative species can subsequently lead to the degradation of organic compounds adsorbed on the surfaces of CAWNs. At the same time, the high electron conductivity of the Ag NPs also helps to improve the photogenerated electron/hole separation process.[46] Being able to absorb visible light (Figure S10) and have stronger adsorption ability, CAWNs showed significantly enhanced photocatalytic activity under visible light.

DOI: 10.1021/acsami.6b14571
ACS Appl. Mater. Interfaces 2017, 9, 7436–7446

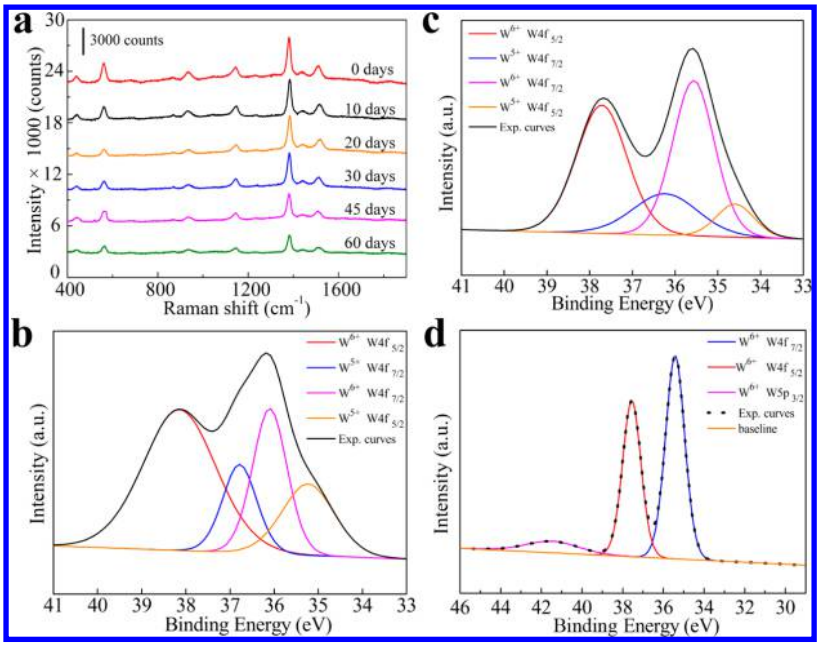

Figure 6. (a) SERS spectra of thiram based on 3D Ag/WO_{3-x} nanostructures collected at different shelf time, and (b–d) represents the W 4f spectra in XPS analysis during different shelf time, 0 days, 30 days, and 60 days, in this order.

The recyclable property is crucial for practical application and needs to be highly valued. If the substrate can be self-cleaning, a renewable substrate can be obtained for further detection. As showed in Figure S11a, this substrate is regenerated each time and the MG solution with the same concentration is subsequently added, and then its SERS signal is detected. The results show that the Raman spectrum of MG is similar at per recyclable detection, indicating that the 3D CAWNs is likely to be developed as a recyclable SERS substrate. Its Raman intensity was slightly deteriorated after five consecutive regenerate experiments (Figure S11b), owing to the degraded hotspots and decreased adsorption capacity. The results demonstrated that the 3D CAWNs could be efficiently regenerated under visible light irradiation and maintain most of its SERS activity (more than 70%). We have also calculated the photocatalytic degradation rate K_1 of absorbed MG molecules, which was estimated to be 0.0462 min^{-1}.

3.5. Rapid and Efficient Detection of Thiram and Its Recycling Performance. Thiram is a typical sulfur-containing pesticide that is often used to prevent fungal diseases in seed and crops. It is moderately toxic by ingestion but is highly toxic if inhaled. As reported in previous reports, the thiram molecule is more likely to form the resonated radical structure after interacting with the Ag NPs, thus leading to the cleavage of S–S bond. This process generates two dimethyl residues that are strongly adsorbed onto Ag NPs via the S–C–S group (a bidentate complex). The adsorption of thiram at the 3D CAWNs provides the best possibility for its identification and detection via SERS techniques.

Figure 5a shows a representative set of SERS spectra, and the corresponding Raman intensity decreases with the decreasing thiram concentration (from 1 μM to 0.5 nM). Even at 0.5 nM, the major peak at 1387 cm^{-1} can also be seen clearly (the magnified view was shown in Figure S12). That is to say, the SERS assay was capable of rapidly detecting thiram as low as 0.5 nM. Several characteristic peaks including 556 cm^{-1}(υ (S–S)), 928 cm^{-1}(υ (CH_3N), υ (C═S)), 1150 cm^{-1}(ρ (CH_3), υ (C–N)), 1387 cm^{-1}(δ (CH_3), υ (C–N)), 1444 cm^{-1}(δ as(CH_3)), and 1508 cm^{-1}(ρ (CH_3), υ (C–N)) can be found within 400–2000 cm^{-1}, which was in good agreement with previous reports.[47,48] The detailed information on peak assignment was shown in Table S2.

The strongest peak at 1387 cm^{-1} can be assigned to the C–N stretching mode and the symmetric CH_3 deformation mode, and this band was used to calibrate the SERS intensity as a function of thiram concentration (Figure 5b). The corresponding quantitative calibration curve was plotted in the inset of Figure 5b, with an excellent linearity of 10^{-9}–10^{-6} M. The calibrated linear regression equation is $\log I_{1387} = (0.412 \pm 0.004) \log C + (6.465 \pm 0.028)$, with a squared correlation coefficient of $R^2 = 0.9862$, and the LOD (S/N = 3) was estimated to be 0.32 nM of thiram. More importantly, it was much lower than the general default MRLs of 0.01 mg/kg in the European Union. Such a low detection limit enables the fabricated SERS substrates to be utilized toward the goal of trace analysis of pesticide residues, which has the potential for a practical application.

Moreover, the thiram molecules can also be eliminated by the self-cleaning CAWNs substrates under the irradiation of visible light. In comparison with the original $WO_{2.72}$ nanochestnuts, the decoration of Ag NPs yielded remarkable photocatalytic activity under visible light excitation.[49] It suggests that the photocatalytic process is assisted by the Ag NPs (Figure S13). Fast and efficient degradation was obtained at the Ag NPs decorated $WO_{2.72}$ nanochestnuts, and the photocatalytic efficiency in 50 min was almost 100%. According to $\ln(C_0/C) = Kt$, the photocatalytic degradation rate K for thiram was estimated to be 0.0648 min^{-1} (C_0 is the concentration of thiram at equilibrium established under dark conditions, C is the concentration of a nondegraded thiram after different irradiation time, and K is the apparent rate constant). In order to investigate the recyclable detection of thiram, the 3D CAWNs SERS substrates were recycled up to six times. As shown in Figure 5c, the SERS signals of thiram almost entirely disappeared after the irradiation of visible light and subsequent rinsing (see curves 2, 4, 6, 8, 10, and 12 in

DOI: 10.1021/acsami.6b14571
ACS Appl. Mater. Interfaces 2017, 9, 7436–7446

Figure 5c). When the thiram was reloaded again with the same concentration, the similar Raman spectrum recovered immediately (see curves 3, 5, 7, 9, and 11 in Figure 5c). In Figure 5d, the result of the study indicated that the as-prepared SERS substrates almost retained its SERS activity (more than 83%) in the five repeated recyclable runs. That is to say, its average Raman intensity was slightly deteriorated by an average of ~3.4% per recyclable detection, which contributed to the degraded hotspots and decreased adsorption capacity. Fortunately, it is sufficient to meet the detection requirements in the qualitative detection of thiram. These results have clearly demonstrated the excellent SERS performance and acceptable reusability of our SERS substrates, which could be used as a feasible recyclable substrate and endure multiple self-cleaning.

3.6. Stability of the CAWNs Substrates. In a real-world application, the stability of the SERS substrates is an important issue.[50] Generally, the excellent plasmonic property of Ag NPs has not been fully utilized because of their poor chemical stability against nonideal chemical environments. We could speculate that the loss probably originated from the oxidation or aggregation of the Ag NPs (Figure S14). However, once the Ag NPs were decorated on the surface of $WO_{2.72}$, no observable changes were found during the shelf life (30 days) compared with that of the fresh ones (Figure 6a). Our results demonstrated that the 3D hierarchical $WO_{2.72}$ scaffolds, acting as an oxygen-defects-rich support, are very effective in guaranteeing the stability of the SERS substrate during their long-term storage in atmospheres at room temperature (Figure 6, panels b-d).

Figure 6 (panels b–d) displays the spectra of W 4f core levels for pristine CAWNs substrates and the substrates stored for 30 and 60 days, respectively. The W 4f core-level spectra could be deconvoluted into two doublets such as W^{5+} and W^{6+}. On the fitting analysis, it was found that the atomic percentage of W^{5+} for pristine Ag/WO_{3-x} was 33.1%, roughly agreeing with the documented values. As the shelf time increased to 30 days, the percentage for W^{5+} decreased to 19.6%. The decreased percentage of W^{5+} indicated that the $WO_{2.72}$ was oxidized into WO_3 partly, and the Ag NPs were protected during this period. In Figure S15, no visible changes were found in the Ag 3d and O 1s XPS, which proves this conclusion. If the shelf time increased to 60 days, the percentage for W^{5+} decreased to 0, and the content of W^{6+} was found to 100%. We can speculate that the $WO_{2.72}$ was oxidized thoroughly and the Ag NPs will no longer be protected. This is consistent with the SERS results between different shelf-time, such as 0 days and 60 days (the SERS intensity begin to degenerate greatly). It can be concluded that the Ag NPs will be protected effectively until the nonstoichiometric $WO_{2.72}$ were oxidized into WO_3 thoroughly in atmospheres at room temperature.

We next assessed the resist oxidation and corrosion resistance of the 3D CAWNs in water. UV–vis characterization was utilized to monitor the plasmonic properties and oxidation process at various soak time. The bare Ag NPs were synthesized and dispersed in water for reference. According to the UV–vis spectra (Figure S16a), we inferred that the bare Ag NPs were easy to be oxidized in water and thus cause the decline of UV–vis spectra. However, when the Ag NPs were decorated on the surface of $WO_{2.72}$, a serial of changeless UV–vis spectra were found (Figure S16b), which indicate its outstanding ability to resist oxidation compared to bare Ag NPs. The results demonstrated that 3D CAWNs exhibited considerable corrosion resistance and resist oxidation in water because the nonstoichiometric $WO_{2.72}$ scaffolds were preferentially oxidized to WO_3. All of these benefited from the protective $WO_{2.72}$ scaffolds. Furthermore, with the soak time increasing, an increasing number of nonstoichiometric $WO_{2.72}$ would be oxidized gradually. A slight blue-shift had begun to appear, which could be attributed to the formation of WO_3 and the interaction between the Ag NPs and their adjacent WO_3 scaffolds.

3.7. Practical Detection of Thiram in Fruit Peels by CAWNs Colloid. The as-synthesized CAWNs were easily isolated and redispersed in appropriate solvents such as water and ethanol (Figure S17). As another very convenient application, the 3D CAWNs substrates were particularly suitable to fabricate the colloid nanoparticles, which can be employed to directly detect the trace pesticides residues at complex surfaces. Some important problems should be solved such as extraction, purification, and sorption on a SERS platform. For example, the thiram is more soluble in nonpolar solvents, thus making it easy to extract from fruits peels.[51] Compared with nanochips SERS substrates, SERS-active CAWNs colloid shows impressive sampling efficiency on peels (Figure S18). First, a droplet of ethanol is dropped onto the spiked fruit peels that are to be probed. It promotes the disassociation of the thiram molecules from peel matrix and increases the analyte concentration on the outer surface of peels. This simple and rapid "extraction" also improves the interactions between the active nanoparticles and the analytes. Then, after the ethanol evaporates naturally, the freshly made active nanoparticle colloid was cast onto the same position. Finally, the Raman spectra were collected from these sites by confocal laser Raman spectrometer until the droplets were nearly dry.

Here, the as-prepared SERS-active CAWNs colloid was employed for the sensitive and rapid detection of thiram in real fruits peels such as carambola and orange. In Figure 7, curves

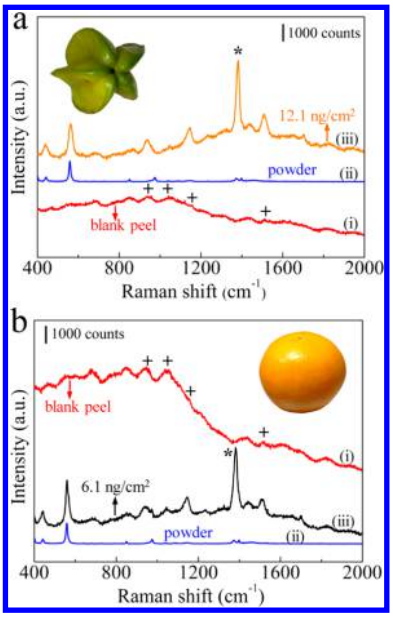

Figure 7. Detection of thiram in real fruits peels, (a) and (b) represents the practical detection of thiram in spiked carambola and orange, respectively; Curves (i), (ii), and (iii) in two figures represent the Raman spectra collected from clean fruit peels, thiram powder, and spiked fruit peels.

DOI: 10.1021/acsami.6b14571
ACS Appl. Mater. Interfaces 2017, 9, 7436–7446

(i) represent Raman spectra of the clean fruit peels without any residues. The characteristic Raman bands at 1157 and 1500 cm^{-1} were clearly found, which were assigned to the carotenoids. Curves (iii) show the SERS spectra collected from the peels of carambola and orange based on SERS-active CAWNs colloid. The Raman spectra of thiram powder were considered as references (curves ii). Also, several differences were found between the SERS spectrum (curves iii) and the normal Raman spectrum of thiram powder (curves ii), such as 1508 and 556 cm^{-1}. The former (1508 cm^{-1}) was greatly enhanced by the SERS substrates but nearly disappeared in thiram powder. The latter (556 cm^{-1}) from thiram powder becomes weaker relatively in the SERS spectrum. These changes suggested that the S−S bond of thiram molecules could be cracked into two dimethylthiocarbamate fragments by the laser irradiation or the potential catalysis effect of 3D CAWNs.

Although the natural background fluorescence interference of biomolecules was observed, the main characteristic peaks of thiram were depicted clearly in the SERS spectra. Importantly, the detection of thiram residues at carambola and orange peels were ∼12.1 and ∼6.1 ng/cm^2, respectively, which was much lower than the MRLs of thiram (0.01−0.1 mg/kg).[52] Besides, the similar detection of food additives, dyes, and other pesticide residues at various fruits peels had been performed successfully. As shown in Figure 8, Sudan I, Sudan III, crystal violet (CV),

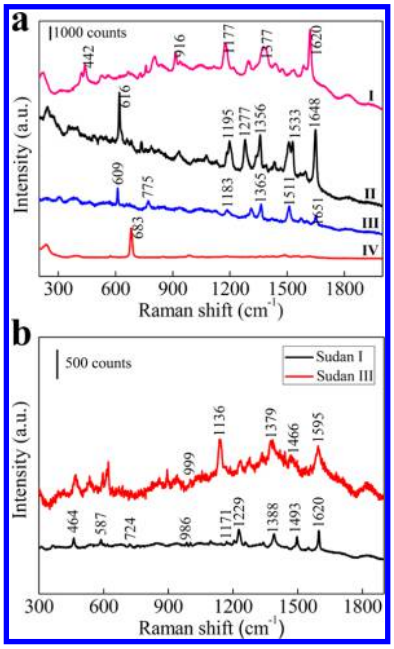

Figure 8. (a) represents the practical detection of (I) CV, (II) MB, (III) R6G, and (IV) melamine by the as-prepared SERS materials and (b) represents the practical detection of Sudan I and Sudan III.

methylene blue (MB), R6G, and melamine were detected easily by our SERS materials. Results of the experiment indicated that the as-prepared SERS materials can detect and identify more analytes and had great potential in food inspection, environment protection, sensing detection, and some other application areas.

4. CONCLUSION

In conclusion, the 3D biomimetic CAWNs were synthesized by a simple hydrothermal method and green in situ redox reaction between weakly reductive $WO_{2.72}$ supports and oxidative metal salt precursors without any additives. Owing to the absence of reductant and other functional additives, the high-quality clean surfaces were obtained with improved signal to background ratio and enhanced sensitivity. A remarkably low concentration of MG down to 2.9×10^{-13} M can readily be discriminated via the developed CAWNs SERS substrates, which was much lower than those traditional analytical approaches. Aside from the ultrahigh sensitivity, the resultant SERS substrates possess an excellent reproducibility (RSD ∼ 7.5%), long-term stability (30 days), and unique recyclable capability by photocatalytic degradation of adsorbed organic probes. With the use of thiram as a model target, the fabricated CAWNs SERS substrates exhibited significant enhancement and pushed the detection limit down to 0.32 nM. The excellent self-cleaning performance indicated that it can be used as a recyclable substrate and endure multiple visible-light cleaning. More significantly, the real-life application is also performed successfully by the detection of thiram in spiked fruits peels using the SERS-active CAWNs colloid. Besides the SERS detection, the substrate obtained in this study might be widely applied in many different fields such as biosensing, photoelectrocatalysis, and medical diagnosis.

■ ASSOCIATED CONTENT

Supporting Information

The Supporting Information is available free of charge on the ACS Publications website at DOI: 10.1021/acsami.6b14571.

Supplementary figures, experimental details, and calculation processes (PDF)

■ AUTHOR INFORMATION

Corresponding Author

*E-mail: yxzhao@mail.xjtu.edu.cn.

ORCID

Yongxi Zhao: 0000-0002-1796-7651

Notes

The authors declare no competing financial interest.

■ ACKNOWLEDGMENTS

The authors thank Wei Gu for making the schemes and figures look pretty. And this work was supported by the National Natural Science Foundation of China (Grants 21475102 and 31671013) and "Young Talent Support Plan" of Xi'an Jiaotong University.

■ REFERENCES

(1) Fleischmann, M.; Hendra, P. J.; McQuillan, A. Raman Spectra of Pyridine Adsorbed at a Silver Electrode. *Chem. Phys. Lett.* **1974**, *26*, 163−166.

(2) Nie, S.; Emory, S. R. Probing Single Molecules and Single Nanoparticles by Surface-Enhanced Raman Scattering. *Science* **1997**, *275*, 1102−1106.

(3) Le Ru, E. C.; Meyer, M.; Etchegoin, P. Proof of Single-Molecule Sensitivity in Surface Enhanced Raman Scattering (SERS) by Means of a Two-Analyte Technique. *J. Phys. Chem. B* **2006**, *110*, 1944−1948.

(4) Moskovits, M. Surface-Enhanced Spectroscopy. *Rev. Mod. Phys.* **1985**, *57*, 783.

(5) Kneipp, K.; Wang, Y.; Kneipp, H.; Perelman, L. T.; Itzkan, I.; Dasari, R. R.; Feld, M. S. Single Molecule Detection Using Surface-Enhanced Raman Scattering (SERS). *Phys. Rev. Lett.* **1997**, *78*, 1667.

(6) Kneipp, K.; Wang, Y.; Kneipp, H.; Itzkan, I.; Dasari, R. R.; Feld, M. S. Population Pumping of Excited Vibrational States by

DOI: 10.1021/acsami.6b14571
ACS Appl. Mater. Interfaces 2017, 9, 7436−7446

Spontaneous Surface-Enhanced Raman Scattering. *Phys. Rev. Lett.* **1996**, *76*, 2444.
(7) Fang, Y.; Seong, N.-H.; Dlott, D. D. Measurement of the Distribution of Site Enhancements in Surface-Enhanced Raman Scattering. *Science* **2008**, *321*, 388−392.
(8) Shen, W.; Lin, X.; Jiang, C.; Li, C.; Lin, H.; Huang, J.; Wang, S.; Liu, G.; Yan, X.; Zhong, Q.; et al. Reliable Quantitative SERS Analysis Facilitated by Core-Shell Nanoparticles with Embedded Internal Standards. *Angew. Chem.* **2015**, *127*, 7416−7420.
(9) Chen, H.-Y.; Lin, M.-H.; Wang, C.-Y.; Chang, Y.-M.; Gwo, S. Large-Scale Hot Spot Engineering for Quantitative SERS at the Single-Molecule Scale. *J. Am. Chem. Soc.* **2015**, *137*, 13698−13705.
(10) Hou, J.; Zhang, H.; Yang, Q.; Li, M.; Jiang, L.; Song, Y. Hydrophilic-Hydrophobic Patterned Molecularly Imprinted Photonic Crystal Sensors for High-Sensitive Colorimetric Detection of Tetracycline. *Small* **2015**, *11*, 2738−2742.
(11) Zhang, K.; Ji, J.; Li, Y.; Liu, B. Interfacial Self-Assembled Functional Nanoparticle Array: a Facile Surface-Enhanced Raman Scattering Sensor for Specific Detection of Trace Analytes. *Anal. Chem.* **2014**, *86*, 6660−6665.
(12) Li, J. F.; Huang, Y. F.; Ding, Y.; Yang, Z. L.; Li, S. B.; Zhou, X. S.; Fan, F. R.; Zhang, W.; Zhou, Z. Y.; Wu, D. Y.; et al. Shell-Isolated Nanoparticle-Enhanced Raman Spectroscopy. *Nature* **2010**, *464*, 392−395.
(13) Wang, P.; Xia, M.; Liang, O.; Sun, K.; Cipriano, A. F.; Schroeder, T.; Liu, H.; Xie, Y.-H. Label-Free SERS Selective Detection of Dopamine and Serotonin Using Graphene-Au Nanopyramid Heterostructure. *Anal. Chem.* **2015**, *87*, 10255−10261.
(14) Liu, Z.; Yang, Z.; Peng, B.; Cao, C.; Zhang, C.; You, H.; Xiong, Q.; Li, Z.; Fang, J. Highly Sensitive, Uniform, and Reproducible Surface-Enhanced Raman Spectroscopy from Hollow Au-Ag Alloy Nanourchins. *Adv. Mater.* **2014**, *26*, 2431−2439.
(15) Tian, C.; Ding, C.; Liu, S.; Yang, S.; Song, X.; Ding, B.; Li, Z.; Fang, J. Nanoparticle Attachment on Silver Corrugated-Wire Nanoantenna for Large Increases of Surface-Enhanced Raman Scattering. *ACS Nano* **2011**, *5*, 9442−9449.
(16) Deng, Z.; Chen, X.; Wang, Y.; Fang, E.; Zhang, Z.; Chen, X. Headspace Thin-Film Microextraction Coupled with Surface-Enhanced Raman Scattering as a Facile Method for Reproducible and Specific Detection of Sulfur Dioxide in Wine. *Anal. Chem.* **2015**, *87*, 633−640.
(17) He, Y.; Su, S.; Xu, T.; Zhong, Y.; Zapien, J. A.; Li, J.; Fan, C.; Lee, S.-T. Silicon Nanowires-Based Highly-Efficient SERS-Active Platform for Ultrasensitive DNA Detection. *Nano Today* **2011**, *6*, 122−130.
(18) Lee, S.; Chon, H.; Lee, J.; Ko, J.; Chung, B. H.; Lim, D. W.; Choo, J. Rapid and Sensitive Phenotypic Marker Detection on Breast Cancer Cells Using Surface-Enhanced Raman Scattering (SERS) Imaging. *Biosens. Bioelectron.* **2014**, *51*, 238−243.
(19) Li, C.-Y.; Meng, M.; Huang, S.-C.; Li, L.; Huang, S.-R.; Chen, S.; Meng, L.-Y.; Panneerselvam, R.; Zhang, S.-J.; Ren, B. "Smart" Ag Nanostructures for Plasmon-Enhanced Spectroscopies. *J. Am. Chem. Soc.* **2015**, *137*, 13784−13787.
(20) Li, J.; Liu, J.; Yang, Y.; Qin, D. Bifunctional Ag@Pd-Ag Nanocubes for Highly Sensitive Monitoring of Catalytic Reactions by Surface-Enhanced Raman Spectroscopy. *J. Am. Chem. Soc.* **2015**, *137*, 7039−7042.
(21) Song, Z.-L.; Chen, Z.; Bian, X.; Zhou, L.-Y.; Ding, D.; Liang, H.; Zou, Y.-X.; Wang, S.-S.; Chen, L.; Yang, C.; et al. Alkyne-Functionalized Superstable Graphitic Silver Nanoparticles for Raman Imaging. *J. Am. Chem. Soc.* **2014**, *136*, 13558−13561.
(22) Lee, S. Y.; Kim, S.-H.; Kim, M. P.; Jeon, H. C.; Kang, H.; Kim, H. J.; Kim, B. J.; Yang, S.-M. Freestanding and Arrayed Nanoporous Microcylinders for Highly Active 3D SERS Substrate. *Chem. Mater.* **2013**, *25*, 2421−2426.
(23) Tang, W.; Chase, D. B.; Rabolt, J. F. Immobilization of Gold Nanorods onto Electrospun Polycaprolactone Fibers via Polyelectrolyte Decoration–a 3D SERS Substrate. *Anal. Chem.* **2013**, *85*, 10702−10709.
(24) Xie, W.; Walkenfort, B.; Schlücker, S. Label-Free SERS Monitoring of Chemical Reactions Catalyzed by Small Gold Nanoparticles Using 3D Plasmonic Superstructures. *J. Am. Chem. Soc.* **2013**, *135*, 1657−1660.
(25) Gómez-Graña, S.; Fernández-López, C.; Polavarapu, L.; Salmon, J.-B.; Leng, J.; Pastoriza-Santos, I.; Perez-Juste. Gold Nanooctahedra with Tunable Size and Microfluidic-Induced 3D Assembly for Highly Uniform SERS-Active Supercrystals. *Chem. Mater.* **2015**, *27*, 8310−8317.
(26) Xie, Y.; Yang, S.; Mao, Z.; Li, P.; Zhao, C.; Cohick, Z.; Huang, P.-H.; Huang, T. J. In situ Fabrication of 3D Ag@ZnO Nanostructures for Microfluidic Surface-Enhanced Raman Scattering Systems. *ACS Nano* **2014**, *8*, 12175−12184.
(27) Tan, Y.; Gu, J.; Xu, W.; Chen, Z.; Liu, D.; Liu, Q.; Zhang, D. Reduction of CuO Butterfly Wing Scales Generates Cu SERS Substrates for DNA Base Detection. *ACS Appl. Mater. Interfaces* **2013**, *5*, 9878−9882.
(28) Xu, Z.; Jiang, J.; Gartia, M. R.; Liu, G. L. Monolithic Integrations of Slanted Silicon Nanostructures on 3D Microstructures and Their Application to Surface-Enhanced Raman Spectroscopy. *J. Phys. Chem. C* **2012**, *116*, 24161−24170.
(29) Gopalakrishnan, A.; Chirumamilla, M.; De Angelis, F.; Toma, A.; Zaccaria, R. P.; Krahne, R. Bimetallic 3D Nanostar Dimers in Ring Cavities: Recyclable and Robust Surface-Enhanced Raman Scattering Substrates for Signal Detection from Few Molecules. *ACS Nano* **2014**, *8*, 7986−7994.
(30) Huang, J.; Ma, D.; Chen, F.; Bai, M.; Xu, K.; Zhao, Y. Ag Nanoparticles Decorated Cactus-Like Ag Dendrites/Si Nanoneedles as Highly Efficient 3D Surface-Enhanced Raman Scattering Substrates Toward Sensitive Sensing. *Anal. Chem.* **2015**, *87*, 10527−10534.
(31) Huang, J.; Chen, F.; Zhang, Q.; Zhan, Y.; Ma, D.; Xu, K.; Zhao, Y. 3D Silver Nanoparticles Decorated Zinc Oxide/Silicon Heterostructured Nanomace Arrays as High-Performance Surface-Enhanced Raman Scattering Substrates. *ACS Appl. Mater. Interfaces* **2015**, *7*, 5725−5735.
(32) Tan, Y.; Gu, J.; Zang, X.; Xu, W.; Shi, K.; Xu, L.; Zhang, D. Versatile Fabrication of Intact Three-Dimensional Metallic Butterfly Wing Scales with Hierarchical Sub-Micrometer Structures. *Angew. Chem.* **2011**, *123*, 8457−8461.
(33) Tan, Y.; Gu, J.; Xu, L.; Zang, X.; Liu, D.; Zhang, W.; Liu, Q.; Zhu, S.; Su, H.; Feng, C. High-Density Hotspots Engineered by Naturally Piled-Up Subwavelength Structures in Three-Dimensional Copper Butterfly Wing Scales for Surface-Enhanced Raman Scattering Detection. *Adv. Funct. Mater.* **2012**, *22*, 1578−1585.
(34) Zhang, B.; Wang, H.; Lu, L.; Ai, K.; Zhang, G.; Cheng, X. Large-Area Silver-Coated Silicon Nanowire Arrays for Molecular Sensing Using Surface-Enhanced Raman Spectroscopy. *Adv. Funct. Mater.* **2008**, *18*, 2348−2355.
(35) Zhao, X.; Zhang, B.; Ai, K.; Zhang, G.; Cao, L.; Liu, X.; Sun, H.; Wang, H.; Lu, L. Monitoring Catalytic Degradation of Dye Molecules on Silver-Coated ZnO Nanowire Arrays by Surface-Enhanced Raman Spectroscopy. *J. Mater. Chem.* **2009**, *19*, 5547−5553.
(36) Li, X.; Chen, G.; Yang, L.; Jin, Z.; Liu, J. Multifunctional Au-Coated TiO_2 Nanotube Arrays as Recyclable SERS Substrates for Multifold Organic Pollutants Detection. *Adv. Funct. Mater.* **2010**, *20*, 2815−2824.
(37) Sun, L.; Zhao, D.; Zhang, Z.; Li, B.; Shen, D. DNA-Based Fabrication of Density-Controlled Vertically Aligned ZnO Nanorod Arrays and Their SERS Applications. *J. Mater. Chem.* **2011**, *21*, 9674−9681.
(38) Xu, L.; Yin, M. L.; Liu, S. F. Ag_x@WO_3 Core-Shell Nanostructure for LSP Enhanced Chemical Sensors. *Sci. Rep.* **2014**, *4*, 6745−6751.
(39) Taylor, C. E.; Garvey, S. D.; Pemberton, J. E. Carbon Contamination at Silver Surfaces: Surface Preparation Procedures Evaluated by Raman Spectroscopy and X-Ray Photoelectron Spectroscopy. *Anal. Chem.* **1996**, *68*, 2401−2408.
(40) Guo, S.; Wang, L.; Wang, E. Templateless, Surfactantless, Simple Electrochemical Route to Rapid Synthesis of Diameter-

DOI: 10.1021/acsami.6b14571
ACS Appl. Mater. Interfaces 2017, 9, 7436−7446

Controlled 3D Flowerlike Gold Microstructure with "Clean" Surface. *Chem. Commun.* **2007**, *30*, 3163−3165.
(41) Nütz, T.; Haase, M. Wet-Chemical Synthesis of Doped Nanoparticles: Optical Properties of Oxygen-Deficient and Antimony-Doped Colloidal SnO_2. *J. Phys. Chem. B* **2000**, *104*, 8430−8437.
(42) Xi, G.; Ye, J.; Ma, Q.; Su, N.; Bai, H.; Wang, C. In situ Growth of Metal Particles on 3D Urchin-Like WO_3 Nanostructures. *J. Am. Chem. Soc.* **2012**, *134*, 6508−6511.
(43) Cong, S.; Yuan, Y.; Chen, Z.; Hou, J.; Yang, M.; Su, Y.; Zhang, Y.; Li, L.; Li, Q.; Geng, F.; Zhao, Z. Noble Metal-Comparable SERS Enhancement from Semiconducting Metal Oxides by Making Oxygen Vacancies. *Nat. Commun.* **2015**, *6*, 7800.
(44) Ghosh, S.; Saha, M.; Paul, S.; De, S. K. Maximizing the Photo Catalytic and Photo Response Properties of Multimodal Plasmonic Ag/WO_{3-x} Heterostructure Nanorods by Variation of the Ag Size. *Nanoscale* **2015**, *7*, 18284−18298.
(45) Le Ru, E.; Blackie, E.; Meyer, M.; Etchegoin, P. G. Surface Enhanced Raman Scattering Enhancement Factors: a Comprehensive Study. *J. Phys. Chem. C* **2007**, *111*, 13794−13803.
(46) Wang, X.; Li, T.; Yu, R.; Yu, H.; Yu, J. Highly Efficient TiO_2 Single-Crystal Photocatalyst with Spatially Separated Ag and F-bicocatalysts: Orientation Transfer of Photogenerated Charges and Their Rapid Interfacial Reaction. *J. Mater. Chem. A* **2016**, *4*, 8682−8689.
(47) Saute, B.; Narayanan, R. Solution-Based Direct Readout Surface Enhanced Raman Spectroscopic (SERS) Detection of Ultra-Low Levels of Thiram with Dogbone Shaped Gold Nanoparticles. *Analyst* **2011**, *136*, 527−532.
(48) Ghosh, S.; Saha, M.; Dev Ashok, V.; Dalal, B.; De, S. K. Tunable Surface Plasmon Resonance in Sn-Doped Zn-Cd-O Alloyed Nanocrystals. *J. Phys. Chem. C* **2015**, *119*, 1180−1187.
(49) Paul, S.; Ghosh, S.; Saha, M.; De, S. K. Enhanced Photophysical Properties of Plasmonic Magnetic Metal-Alloyed Semiconductor Heterostructure Nanocrystals: a Case Study for the Ag@Ni/$Zn_{1-x}Mg_xO$ System. *Phys. Chem. Chem. Phys.* **2016**, *18*, 13092−13107.
(50) Yang, Y.; Liu, J.; Fu, Z.-W.; Qin, D. Galvanic Replacement-Free Deposition of Au on Ag for Core-Shell Nanocubes with Enhanced Chemical Stability and SERS Activity. *J. Am. Chem. Soc.* **2014**, *136*, 8153−8156.
(51) Liu, B.; Han, G.; Zhang, Z.; Liu, R.; Jiang, C.; Wang, S.; Han, M.-Y. Shell Thickness-Dependent Raman Enhancement for Rapid Identification and Detection of Pesticide Residues at Fruit Peels. *Anal. Chem.* **2012**, *84*, 255−261.
(52) Chen, J.; Huang, Y.; Kannan, P.; Zhang, L.; Lin, Z.; Zhang, J.; Chen, T.; Guo, L. Flexible and Adhesive Surface Enhance Raman Scattering Active Tape for Rapid Detection of Pesticide Residues in Fruits and Vegetables. *Anal. Chem.* **2016**, *88*, 2149−2155.

DOI: 10.1021/acsami.6b14571
ACS Appl. Mater. Interfaces 2017, 9, 7436−7446